

Repeatable, room-temperature processed baroplastic/carbon nanotube composites for electromagnetic interference shielding

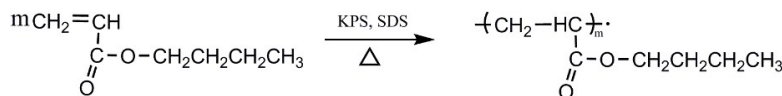
Zhi Lv,^a Chuan-Li Jia,^a Xu Ji,^b Ding-Xiang Yan,^{*a} Jun Lei,^{*a} Zhong-Ming Li^a

^aCollege of Polymer Science and Engineering, State Key Laboratory of Polymer Materials Engineering, Sichuan University, Chengdu 610065, China. Email: yandingxiang@scu.edu.cn; leijun@scu.edu.cn

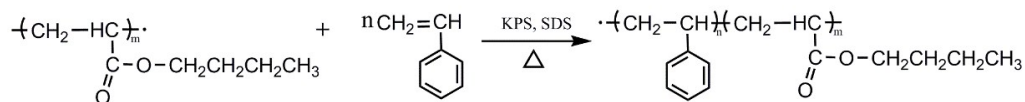
^bCollege of Chemical Engineering, Sichuan University, Chengdu, 610065, China

Polymerization

PBA core



PBA@PS core-shell polymer



Scheme S1 Two-stage emulsion polymerization of poly(n-butyl acrylate) @ polystyrene (PBA@PS) core shell polymer.

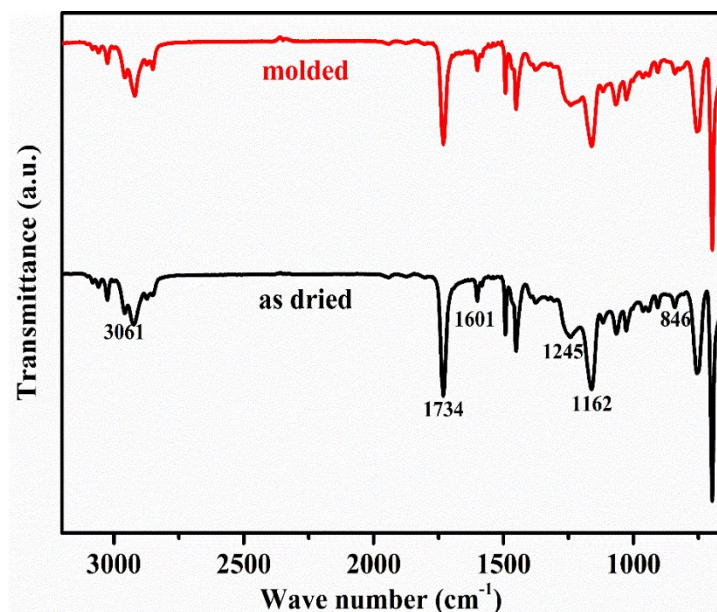


Fig. S1 FTIR spectrum of the as dried PBA@PS and the molded samples.

A typical FTIR spectrum is shown in Fig. S2. A strong carbonyl peak at 1734 cm^{-1} indicates the presence of PBA. Peaks at 1162 and 1245 cm^{-1} corresponded to the asymmetrical vibration of C-O-C attached to PBA imply the same results. Peaks at 3061 , 3026 , and 1601 cm^{-1} corresponded to the benzene ring of PS indicate the presence of PS component. The number-average molecular weight (M_n) and weight-average molecular weight (M_w), measured by GPC test are $\sim 53,000$ and $\sim 135,000\text{ g/mol}$, respectively. These results show a successful synthesis of PBA@PS core shell polymer.

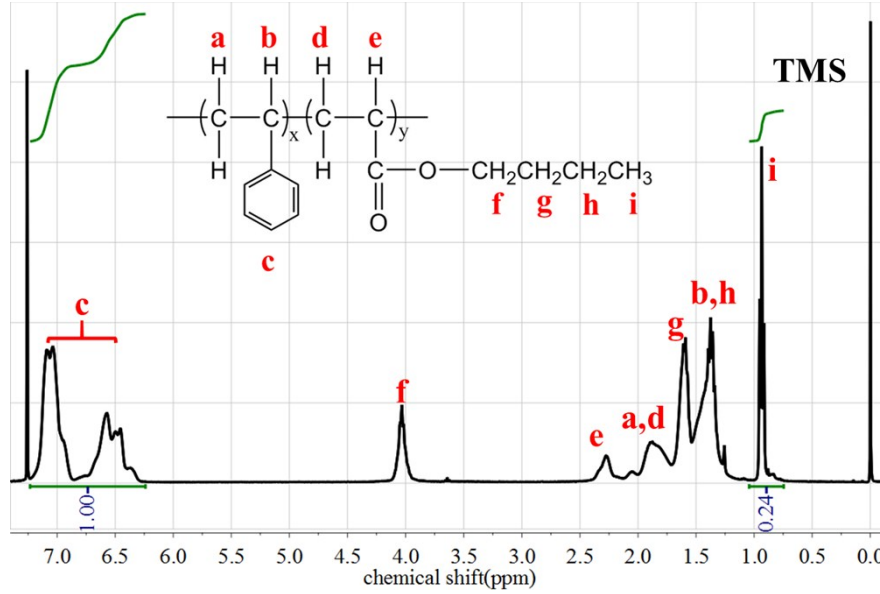


Fig. S2 Typical ^1H NMR spectrum of the as dried PBA@PS granules.

Coverage of the PBA core by the PS shell appears completely for higher PS content samples (above 50 wt% PS), for which a powdery product is obtained upon precipitation.¹ So that composition of the PBA@PS takes great role in the morphology of the PBA@PS granules. NMR test was performed to calculate the core-shell composition of the as dried PBA@PS granules. Composition of the resulting particles is 67 wt% PS (over 50 wt%), calculated from the integral ratio of characteristic resonances for PS at 6.3-7.2 ppm (styrene aromatic) and the core polymer at 0.9 ppm (methyl protons of BA) via equation (1).²

$$\text{PS wt\%} = \frac{104 \int \text{PS}_{\text{Ar}}/5}{(104 \int \text{PS}_{\text{Ar}}/5) + (128 \int \text{PBA}_{\text{CH}_3}/3)} \quad (1)$$

where $\int \text{PS}_{\text{Ar}}$ is the integral of the aromatic protons (c in Fig. S2) attributed to polystyrene, and $\int \text{PBA}_{\text{CH}_3}$ is the integral of the methyl protons (i in Fig. S2) of the PBA of PBA@PS.

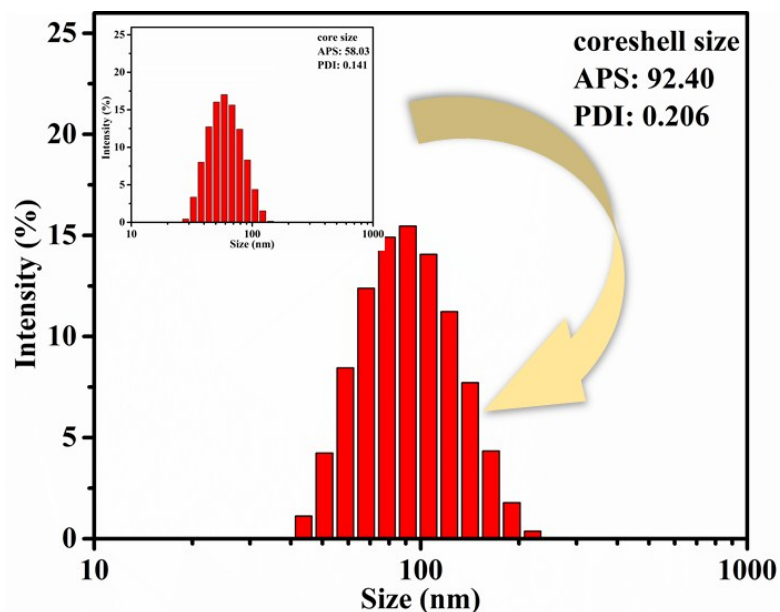


Fig. S3 Particle size distribution of PBA core (inset) and PBA@PS core-shell.

Fig. S3 shows the representative particle size distribution of PBA core and PBA@PS core-shell nanoparticles. As determined by dynamic light scattering (DLS), APS increases from 58 nm to 92 nm after adding the styrene monomer in the second polymerization stage. Both histograms indicate very narrow particle size distributions and the final APS is comparable to the SEM result.

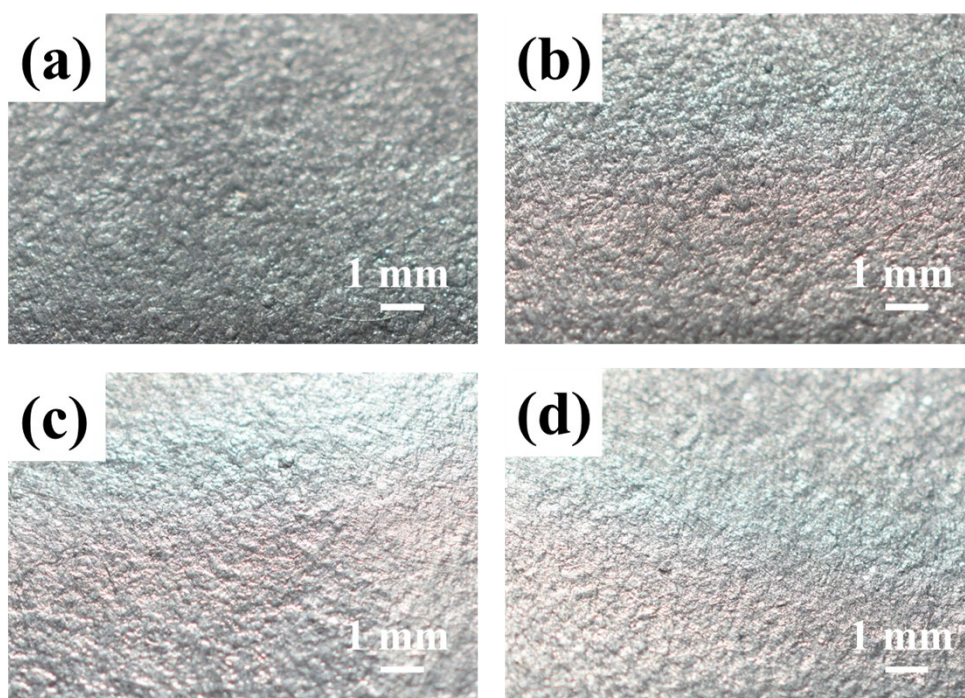


Fig. S4 Photographs of surfaces of CNT/PBA@PS composite via digital camera (Nikon d7000) with 3.0 wt% CNT loading processed the first (a), fourth (b), seventh (c) and tenth (d) cycle at 25 °C under a pressure of 300 MPa.

Fig. S4 shows the photographs of the surfaces of CNT/PBA@PS composites after various processing cycles. It is obvious that the remolded composites (Fig. S4b, c and d) maintain the similar surfaces in comparison to that for the 1C specimen (Fig. S4a).

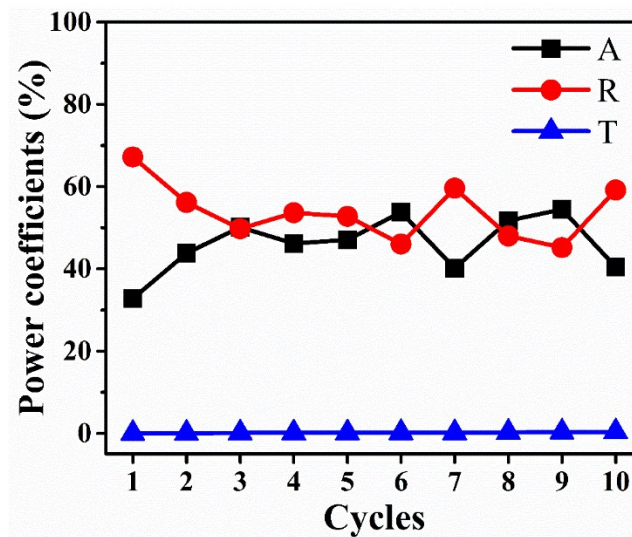


Fig. S5 T, R, and A of the CNT/PBA@PS composites as a function of processing cycles.

Considering that SE_A is calculated as $-10\log[T/(1-R)]$ and shows the EMI shielding only of the electromagnetic wave portion capable of entering inside the composite, we also explore the EMI shielding mechanisms of the CNT/PBA@PS composites based on the power coefficients (transmission coefficient (T), reflection coefficient (R), and absorption coefficient (A)). Fig. S5 shows T , R , and A of the CNT/PBA@PS composites as a function of processing cycles. As processing cycles increase, T increases slightly, indicating the stable EMI shielding ability. R exhibits a decrease with processing cycle, which should be attributed to the impedance match at interfaces induced by the low conductivity of the CNT/PBA@PS composites. A undergoes a process of first increase

and then fluctuation. It is worth noting that when the processing cycles increase, A and R are almost the same, while SE_A is higher than SE_R , among all cycles. Such distinction demonstrates again that A and R are quantitative characteristics of whole incident electromagnetic wave on the composite, while SE_A and SE_R represent the electromagnetic wave entering inside the composite. Since reflection occurs before absorption, the large contribution of SE_A to $EMI SE$ indicates that the CNT/PBA@PS composite maintains the absorption-dominated shielding mechanism of electromagnetic wave inside the composite.

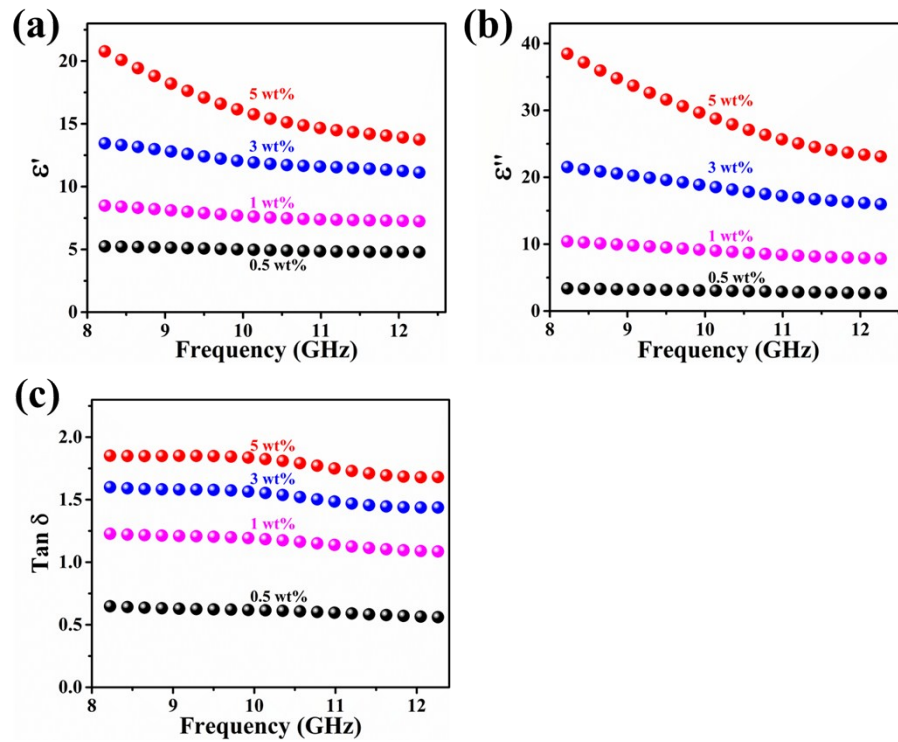


Fig. S6 Electromagnetic characteristics of CNT/PBA@PS composites with variation of CNT content in the 8.2-12.4 GHz: (a) real permittivity, (b) imaginary permittivity and (c) loss tangent.

The real permittivity (ϵ' , known as dielectric constant) represents the storage of electrical energy, whereas imaginary permittivity (ϵ'' , known as dielectric loss) corresponds to the dissipation of electrical energy. Both the ϵ' and ϵ'' of the

CNT/PBA@PS composites increase with the increase of CNT content across the whole X-band, suggesting a gradually increased efficiency in storing and attenuating the electrical energy for the CNT/PBA@PS composites. For example, the ϵ' of samples increase from 4.9 to 15.5 and the ϵ'' of samples increase from 3.0 to 28.1 at the frequency of 10.3 GHz, which is mainly attributed to the higher electrical conductivity with increased CNT content. The loss tangent ($\tan \delta = \epsilon''/\epsilon'$) was applied to characterize the absorption and dissipation of the incident electromagnetic wave and was shown in Fig. S6c. The $\tan \delta$ for the CNT/PBA@PS composites exhibits a significant increase with increased CNT content. For example, the $\tan \delta$ value of the 5.0 wt% CNT/PBA@PS composite can reach 1.81 at the frequency of 10.3 GHz, which indicates a strong dissipation of electromagnetic wave as heat.

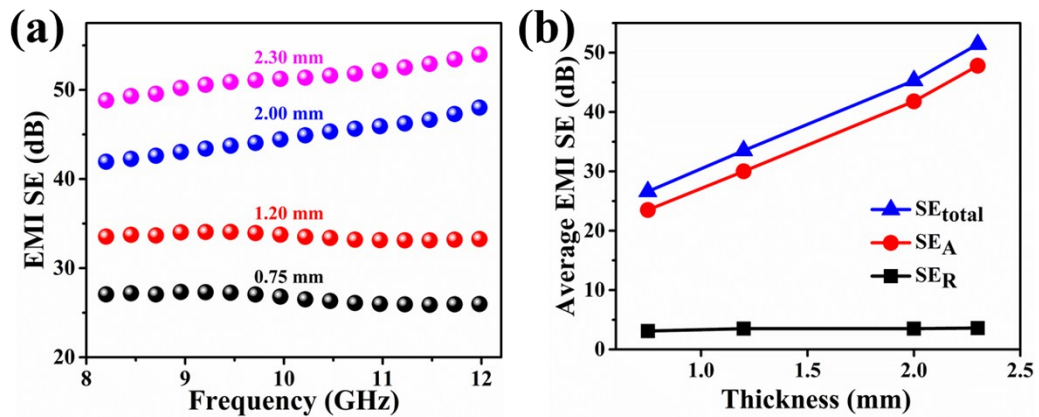


Fig. S7 (a) EMI SE for the CNT/PBA@PS composites with different specimen thicknesses at the CNT loading of 5.0 wt%. (b) Comparison of average SE_{total} , SE_A and SE_R .

The composite thickness plays an important role in the EMI shielding performance for a shielding material. The $EMI SE$ of the 5.0 wt% CNT/PBA@PS composite specimens with varying thickness is thus characterized, as presented in Fig. S7a. Specimens with larger thickness display more striking EMI shielding performance. As

shown in Fig. S7b, it should be emphasized that the SE_A of the composite increases with the increase of thickness while SE_R remains almost constant. The absorption-dominated shielding mechanism is proven again because of the dominant contribution of SE_A that is as high as 88% of the SE_{total} , for the thicknesses varying from 0.75 to 2.30 mm.

References

- 1 J. A. Gonzalez-Leon, S. W. Ryu, S. A. Hewlett, S. H. Ibrahim and A. M. Mayes, *Macromolecules*, 2005, **38**, 8036-8044.
- 2 T. G. Wright, H. Pfukwa and H. Pasch, *Anal. Chim. Acta*, 2015, **892**, 183-U203.